Article

An Underlying Mechanism of Dual Wnt Inhibition and AMPK Activation: Mitochondrial Uncouplers Masquerading as Wnt Inhibitors

Wen Zhang, Vitaliy M Sviripa, Liliia Kril, Tianxin Yu, Yanqi Xie, William Brad Hubbard, Pat Sullivan, Xi Chen, Chang-Guo Zhan, Yang Yang-Hartwich, B. Mark Evers, Brett Spear, Roberto Gedaly, David S. Watt, and Chunming Liu

J. Med. Chem., **Just Accepted Manuscript** • DOI: 10.1021/acs.jmedchem.9b01685 • Publication Date (Web): 27 Nov 2019

An Underlying Mechanism of Dual Wnt Inhibition and AMPK Activation: Mitochondrial Uncouplers Masquerading as Wnt Inhibitors

Wen Zhang[1,2], Vitaliy M. Sviripa[3,4], Liliia M. Kril[1,2,3], Tianxin Yu[1,2], Yanqi Xie[1,2], W. Brad Hubbard[5], Patrick G. Sullivan[5], Xi Chen[4], Chang-Guo Zhan[4], Yang Yang-Hartwich[6], B. Mark Evers[2,7], Brett T. Spear[2,8], Roberto Gedaly[2,7,9], David S. Watt[1,2,3*] and Chunming Liu[1,2*]

[1]Department of Molecular and Cellular Biochemistry, College of Medicine, University of Kentucky, Lexington, KY 40536

[2]Lucille Parker Markey Cancer Center, University of Kentucky, Lexington, KY 40536

[3]Center for Pharmaceutical Research and Innovation, College of Pharmacy, University of Kentucky, Lexington, KY 40536

[4]Department of Pharmaceutical Sciences, College of Pharmacy, University of Kentucky, Lexington, KY 40536

[5]Department of Neuroscience, College of Medicine, University of Kentucky, Lexington, KY 40536

[6]Department of Obstetrics, Gynecology and Reproductive Sciences, Yale School of Medicine LSOG 209, 375 Congress Avenue, New Haven CT 06510

[7]Department of Surgery, College of Medicine, University of Kentucky, Lexington, KY 40536

[8]Department of Microbiology, Immunology and Molecular Genetics, University of Kentucky, Lexington, KY 40536

[9]Transplant Center, College of Medicine, University of Kentucky, Lexington, KY 40536

*Correspondence to: chunming.liu@uky.edu or dwatt@uky.edu

Abstract

The importance of upregulated Wnt signaling in colorectal cancers led to efforts to develop inhibitors that target β-catenin in this pathway. We now report that several "Wnt inhibitors" that allegedly target β-catenin actually function as mitochondrial proton uncouplers that independently activate AMPK and concomitantly inhibit Wnt signaling. As expected for a process in which mitochondrial uncoupling diminishes ATP production, a mitochondrial proton uncoupler, FCCP, and a glucose metabolic inhibitor, 2-DG, activated AMPK and inhibited Wnt signaling. Also consistent with these findings, a well-known "Wnt inhibitor", FH535, functioned as a proton uncoupler, and in support of this finding, the *N*-methylated analog, 2,5-dichloro-*N*-methyl-*N*-(2-methyl-4-nitrophenyl)benzenesulfonamide (FH535-M) was inactive as an uncoupler and Wnt inhibitor. Apart from suggesting an opportunity to develop dual Wnt inhibitors and AMPK activators, these findings provide a cautionary tale that claims for Wnt inhibition alone require scrutiny as possible mitochondrial proton uncouplers or inhibitors of the electron transport chain.

Introduction

Aberrant activation of Wnt signaling is a hallmark of many human cancers, particularly colorectal cancer (CRC), and the development of inhibitors that target this pathway and the re-purposing of non-cancer related, FDA-approved drugs that target this pathway represent promising venues for therapeutic advances in cancer treatment [1-5]. The Wnt inhibitors in current use include "off-label" drugs and new agents now under evaluation in Phase 1/2 clinical trials [2, 4, 6]. The mechanisms by which these agents affect the Wnt signaling pathway are often unclear, and efforts to understand these events at a biochemical level will facilitate the development of future Wnt inhibitors.

In the absence of ligands that trigger Wnt signaling, β-catenin undergoes sequential phosphorylation by casein kinase-1 alpha (CK1α) and glycogen synthase kinase-3 (GSK3) in the Axin/Adenomatous Polyposis Coli complex (Axin/APC) [7] to furnish phosphorylated β-catenin. In normal cells, phosphorylated β-catenin undergoes ubiquitination by β-Transducin Repeat Containing E3 Ubiquitin Protein Ligase (β-TrCP) and subsequent proteasomal degradation [2-4, 7, 8]. In colorectal cancer cells, mutations in either β-catenin or APC render this phosphorylation-ubiquitination-degradation sequence dysfunctional, and either β-catenin phosphorylation or β-TrCP-mediated degradation fail. These outcomes lead to aberrant β-catenin accumulation and the translocation of undesired levels of β-catenin to the nucleus [3, 9]. In the nucleus, these augmented levels of β-catenin bind to co-activators, including the T-cell factor/lymphoid enhancer factor

(TCF/LEF), induce transcription of Wnt-target genes, such as c-Myc and cyclin D1, and promote undesired growth [3].

The complexity of the Wnt pathway lends itself to the development of inhibitors that target various stages of these signaling events. High-throughput-screening methods using stable cell lines containing Wnt reporter genes find frequent application for siRNA or in small molecule screening [10, 11]. Porcupine inhibitors [12], IWP-2 or LGK974, block the secretion of Wnt ligands that initiate the signaling cascade and promote β-catenin degradation. Tankyrase inhibitors [13], XAV939 or IWR-1, stabilize Axin and also promote β-catenin degradation. Other inhibitors, such as ICG-001, bind and inhibit CREB-binding Protein (CBP), a transcriptional co-activator of the β-catenin/TCF complex, and inhibit Wnt target gene expression [14]. In contrast, several, alleged Wnt inhibitors lack direct targets or clear mechanisms but find widespread use by many investigators in research focused on understanding the Wnt pathway or cancer biology.

We studied alleged Wnt inhibitors in several chemical classes (*e.g.*, *N,N*-diarylureas, *N*-aryl benzenesulfonamides), but we failed, despite considerable effort, to elucidate precise biological targets associated *directly* with the Wnt signaling pathway using biologically active biotinylated analogs and pull-down assays [15, 16]. For example, after screening a library of more than 5,000 compounds using a stable HEK293T cell line containing a modified TOPFlash reporter we identified 1-(1,1,1,4,4,4-hexafluoro-2-(trifluoromethyl)butan-2-yl)-3-(5-(trifluoromethyl)-1,3,4-thiadiazol-2-yl)urea (FTU-11) **(Fig. 1A)** as a potential Wnt inhibitor. We noted that FTU-11 resembled another

fluorinated urea, 1-(4-(trifluoromethyl)phenyl)-3-(3,4,5-trifluorophenyl)urea (FDN-4E) (**Fig. 1A**), reported to function as an AMPK activator [17, 18]. Our chance observations that FDN-4E also inhibited Wnt signaling and that FTU-11 also activated AMPK signaling suggested a common mechanism for urea-mediated, Wnt inhibition and AMPK activation. As an additional example, the *N*-aryl benezenesulfonamide, 2,5-dichloro-*N*-(2-methyl-4-nitrophenyl)benzenesulfonamide (FH535), reported as an inhibitor of both β-catenin in the Wnt signaling pathway and the Peroxisome Proliferator-activated Receptor (PPAR) [19], also activated AMPK. A confluence of screening, and analog development along several lines led a fortuitous intersection of experiments in which we recognized a linkage among the Wnt pathway, AMPK activation, and oxidative phosphorylation. We identified several *soi-disant* Wnt inhibitors that actually function as proton uncouplers or electron-transport inhibitors.

Results and Discussion

To identify novel Wnt regulators by high throughput screening, a stable HEK293T cell line containing the TOPFlash reporter was established [5]. To identify Wnt inhibitors that targeted molecular events downstream of β-catenin, we treated these cells with lithium chloride to inhibit GSK3 and to stabilize β-catenin. Screening a library previously available from the Drug Discovery Center at University of Cincinnati (Cincinnati, OH, USA) led to the identification of FTU-11 (**Fig. 1A**) that inhibited Wnt signaling at a 0.5 μM concentration (96-well assay using stable cell line) (**Fig. 1B**). FTU-11 possessed structural features that resembled another highly fluorinated urea, FDN-4E (**Fig. 1A**), that functioned as a potent AMPK activator and repressed the growth of CRC cells [17, 18]. A comparison study of FTU-11 and FDN-4E using the luciferase assay revealed that FDN-4E also inhibited Wnt signaling (24-well assay using stable cell line) (**Fig. 1C**). We also validated the results by transient transfection of Super 8x TOPFlash or 8x FOPFlash into HEK293T cells. Both FTU-11 and FDN-4E inhibited TOPFlash but not FOPFlash activity (**Fig. 1D**). Since the results from the stable and transient transfection are compatible, we used stable cell lines for all of the other experiments. In addition, the reporter activity, FTU-11 and FND-4E also inhibited the proliferation of colon cancer cells at sub-micromolar concentrations (**Fig. 2A**) and inhibited Wnt target genes in three CRC cell lines (**Fig. 2B**).

Most importantly, we observed that FTU-11 functioned as an AMPK activator equal in potency to FDN-4E, and as expected for an AMPK activator, FTU-11 inhibited acetyl-

CoA carboxylase (ACC) that was subject to regulation by phosphorylated AMPK (**Fig. 3**). Taken together, these findings suggested a linkage between AMPK activation and the inhibition of Wnt signaling. We probed this relationship using a series of AMPK inhibitors and activators as well as inhibitors of the Wnt pathway in which we accepted at face value the assertions in the literature that these Wnt inhibitors and AMPK activators had exclusive selectivity for one of these targets. As a working hypothesis, we assumed a direct relationship in which FTU-11 and FDN-4E disrupted some cellular process that triggered AMPK activation. The phosphorylated AMPK in turn served as an inhibitor of the ATP-dependent Wnt pathway.

We treated HEK293T cells containing a modified TOPFlash reporter simultaneously with either FTU-11 or FDN-4E and with a potent AMPK inhibitor, 4-(2-(4-(3-(pyridin-4-yl)pyrazolo[1,5-a]pyrimidin-6-yl)phenoxy)ethyl)morpholine, known commonly as "Compound C" [20]. If the inhibition of Wnt signaling required activated, phosphorylated AMPK, as proposed in our hypothesis, then Compound C should rescue the Wnt signaling inhibited by either FTU-11 or FDN-4E. Compound C inhibited ACC phosphorylation (*i.e.*, conversion to its inactive form), as expected (**Fig. 4A**), but it had no effect on either the FTU-11-mediated or FDN-4E-mediated Wnt inhibition (**Fig. 4B**). Next, we treated HEK293T cells containing a modified TOPFlash reporter with an AMPK activator, 4-hydroxy-3-(2'-hydroxy-[1,1'-biphenyl]-4-yl)-6-oxo-6,7-dihydrothieno[2,3-*b*]pyridine-5-carbonitrile (A769662) (**Fig. 4C**), but unlike the results using FTU-11 and FDN-4E, the direct AMPK activator, A769662 [21-23], did not inhibit

Wnt signaling (**Fig. 4B**). Taken together, these results suggested that the ureas, FTU-11 and FDN-4E, inhibited Wnt signaling through an AMPK-independent mechanism.

We hypothesized that either FTU-11 or FDN-4E affected a cellular process that altered Wnt signaling and *independently* triggered the activation of the AMPK energy sensor. We tested well-known Wnt inhibitors, such as (*6S,9aS*)-*N*-benzyl-6-(4-hydroxybenzyl)-8-(naphthalen-1-ylmethyl)-4,7-dioxohexahydro-2H-pyrazino[1,2-*a*]pyrimidine-1(6*H*)-carboxamide (ICG-001) and FH535 [14, 19]. These compounds had dramatically different effects on AMPK activation. ICG-001 only inhibited Wnt signaling but had no effect on AMPK (data not shown), and in contrast, FH535 not only inhibited Wnt signaling (**Fig. 4D**) but also induced AMPK phosphorylation and ACC phosphorylation (**Fig. 4E**). Since ICG-001 was a well-characterized Wnt inhibitor with a specific target, namely the CREB Binding Protein (CBP) [14], we concluded that FTU-11 and FH535 activated AMPK through Wnt-independent mechanisms. In addition, we detected AMPK activation within 15 min of treatment with FH535. This rapid response was inconsistent with AMPK regulation mediated by Wnt transcription. In conclusion, AMPK activation was an unlikely a consequence of Wnt inhibition.

Since either FTU-11 or FH535, but not A769662, inhibited Wnt signaling, we concluded that these *N,N*-diarylureas *indirectly* activated AMPK through a mechanism that altered AMP/ATP ratio. To confirm this point, we analyzed ATP production in FTU-11-treated and FH535-treated cells using a Seashorse XF Analyzer. As a control, we selected a well known mitochondrial uncoupler, *N*-(4-(trifluoromethoxy)phenyl)carbonohydrazonoyl

dicyanide (FCCP) [24], and we found that FTU-11, FH535 and FCCP decreased the rates of ATP production in mitochondria (**Fig. 5A**). As expected, the decrease in mitochondrial ATP production led to concomitant increase in glycolytic ATP production and AMPK activation. These results suggested that these compounds induced AMPK activation by inhibiting mitochondrial function.

FCCP represented a potent, mitochondrial uncoupler that translocated protons across the mitochondrial inner membrane, decreased oxidative phosphorylation that provided ATP and increased oxygen consumption rate (OCR) as a means of compensating for the increased pH in the intermembrane space. FCCP possessed both a hydrophobic substructure and an ionizable nitrogen-hydrogen bond with a pK_a sufficient to function as a transmembrane proton transporter. Since uncouplers reduced membrane potential, we analyzed the effect of FTU-11 on mitochondrial membrane potential using tetramethylrhodamine methyl ester (TMRM) staining and found that FTC-11 significantly reduced the membrane potential of mitochondria (**Fig. 5B**). FDN-4E and FH535 had similar effects (data not shown).

A previous study indicated that FH535 affected mitochondria respiration, but the exact mechanism was unclear [25]. The above data suggested that the ureas in this study and other, *soi-disant* Wnt inhibitors functioned as mitochondrial proton uncouplers. We next analyzed the effects of these compounds on OCR using Seashorse XF Analyzer, with FCCP as a control (**Figs. 5C and D**). Oligomycin (Oligo) inhibited ATPase and thus inhibited OCR [24]. FCCP, FTC-11 and FH535 uncoupled mitochondrial

oxidation/phosphorylation (OXPHOS) and increased OCR inhibited by oligomycin (**Figs. 5E and F**). Rotenone and antimycin A blocked the increase in OCR by inhibiting electron-transport Complexes I and III, respectively [24].

In the uncoupling assay, FH535 had the same function as the standard mitochondrial uncoupler, FCCP. As was the case for FCCP, FH535 also possessed a hydrophobic substructure and an ionizable, nitrogen-hydrogen bond that participated in proton translocation. To confirm this point, we replaced this "active" hydrogen with a methyl group (**Fig. 6A**), and as expected, we found that the *N*-methyl analog, 2,5-dichloro-*N*-methyl-*N*-(2-methyl-4-nitrophenyl)benzenesulfonamide (FH535-M), no longer functioned as a mitochondrial uncoupler (**Fig. 6B**) and did not activate AMPK or inhibit Wnt (data not shown). Furthermore, we synthesized FH535 analogs and identified 2,5-dichloro-*N*-(4-nitronaphthalen-1-yl)benzenesulfonamide analog, which we called Y3 (**Fig. 6A**), that strongly activated AMPK and inhibited Wnt signaling (**Fig. 6C and D**). Just as in the case of FH535 and FH535-M, the methylated version of Y3, 2,5-dichloro-*N*-methyl-*N*-(4-nitronaphthalen-1-yl)benzenesulfonamide (Y3-M) (**Fig. 6A**), failed as a mitochondrial uncoupler (data not shown) and led to neither AMPK activation (**Fig. 6C**) or Wnt inhibition (**Fig. 6D**).

The calculated pK_a values for FH535 and Y3 using the ACD/pK_a DB (version 11.1) software (Advanced Chemistry Development, Inc., Toronto, Ontario, Canada) were 5.83 and 5.39, respectively, and the calculated pK_a values for FH535 and Y3 using the ChemAxon (version 19.18) software (ChemAxon, Inc., Cambridge, MA) were 6.69 and

6.46, respectively. In support of the validity of these pK_a values, the calculated values for another sulfonamide, trifluoromethanesulfonamide ($CF_3SO_2NH_2$), using these same two programs were 6.37 and 6.19, respectively, and these values compared well with the experimentally determined value [26] of 6.3. Based on the reported pH values [27] for the intermembrane space (pH 6.88±0.09) and the mitochondrial matrix (pH 7.78±0.17) and assuming the release of these uncouplers into these two compartments and not simply the retention in the inner membrane, the ChemAxon pK_a values predicted that the percentages of the protonated forms of FH535 in the hydronium ion-rich intermembrane space and the mitochondrial matrix were 39% and 8%, respectively (**Fig. 7A**). In the same fashion, the percentages of the protonated forms of Y3 in the hydronium ion-rich intermembrane space and the mitochondrial matrix were 28% and 5%, respectively.

A model for proton translocation entails the transport of the uncoupler and the conjugate base of the uncoupler across the inner mitochondrial membrane. As suggested diagrammatically (**Fig. 7A**), the inner membrane possesses several transporters for the translocation of other anionic species (*e.g.*, P_i, ADP), and these channels may participate in translocating the conjugate base [28]. In summary, these calculated pK_a values and pH values for the intermembrane space and matrix of mitochondria were consistent with both FH535 and Y3 retaining reasonable, equilibrium concentrations of protonated and unprotonated forms sufficient to translocate protons across the inner membrane. In addition, FH535 and Y3 possessed calculated log P values (*i.e.,* 5.83 and 5.39, respectively), and these values were similar to other mitochondrial proton uncouplers, again consistent with representing FH535 and Y3 as weak acids possessing the necessary

lipophilicity to accomplish uncoupling. These results further supported that the mitochondrial proton uncoupling activity of these compounds contributed to their activities as AMPK activators and Wnt inhibitors.

Since the above studies were performed in human cell lines, it was not clear whether the test compounds targeted mitochondria directly, or indirectly through cell signaling pathways, including the Wnt signaling pathway. To address this question, we performed uncoupling assay using purified mitochondria from mouse livers. Similar to the results in cell lines, the OCR was blocked by oligomycin rescued by control proton uncoupler, FCCP. FH535 and Y3 also increased OCR in dose-dependent manner, but as expected, the methylated analogs, FH535-M and Y3-M were inactive as mitochondrial proton uncouplers (**Figs. 7B, 7C**). Although we cannot rule out the possibility that these compounds may also have a mitochondrial-independent function, the experiments with purified mitochondria suggested that these "Wnt inhibitors" directly target mitochondria as proton uncouplers.

To test the hypothesis that the uncoupling effects inhibited Wnt signaling, we also analyzed a classic mitochondrial proton uncoupler, FCCP, and found that FCCP strongly activated AMPK (**Fig. 8A**) and inhibited Wnt signaling (**Fig. 8B**). We then tested numerous inhibitors in the Seahorse assay, including oligomycin, rotenone and antimycin and found that all of them inhibited oxidative phosphorylation, activated AMPK and inhibited Wnt signaling (data not shown), an observation again consistent with the inhibition of Wnt signaling by reduced ATP production. To test further this hypothesis,

we treated cells with a metabolically inert, glucose analog, 2-deoxy-D-glucose (2-DG), to reduce ATP levels by inhibiting glucose metabolism [29], and as expected 2-DG activated AMPK (**Fig. 8C**), inhibited Wnt signaling (**Fig. 8D**) and reduced ATP levels in treated cells (**Fig. 8E**). We analyzed the β-catenin levels in LS174T cells. LiCl treatment increased both total and nucleus β-catenin. FTU-11 and FH535 treatment reduced β-catenin induced by LiCl (**Fig. 8F**), suggesting that uncouplers may affect β-catenin protein synthesis or nuclear localization.

Conclusions

Many steps in the Wnt signaling pathway, including β-catenin nuclear import and chromatin remodeling, are ATP-dependent [3, 30, 31]. We found the FTU-11 and FH535 reduced β-catenin levels in LS174T cells (**Fig. 8F**), consisted with ATP requirements for β-catenin protein synthesis or nuclear localization. Other reports described ATP-dependent steps in Wnt signaling. For example, the ATP-dependent chromatin remodeling protein, Brg1, bound to β-catenin and actived the transcription of Wnt-target genes [30]. Deletion of the ATPase domain of Brg1 inhibited Wnt signaling. Loss of Brg1 attenuated Wnt signaling and prevent Wnt-dependent tumorigenesis in the intestines [32]. A recent paper suggested that impaired mitochondrial ATP production inhibited Wnt signaling *via* an induction of ER stress [33]. Wnt signaling also regulates mitochondria dynamics and membrane potential in a subset of cancers [34]. Although ATP is not specifically required for Wnt signaling, this study illuminated the linkage between this ATP requirement and claims that some compounds, previously identified as *direct* Wnt

inhibitors, in fact function as either inhibitors of mitochondrial oxidative phosphorylation or the electron transport chain. This study not only suggested a need to re-examine some of these prior claims but also suggested a new strategy for inhibiting Wnt signaling in the development of new antineoplastic agents for cancer treatment. Many agents that function as AMPK activators may also act as Wnt inhibitors and provide an impetus to examine connections in which drugs for treating metabolic disorders find a potential application in cancer therapeutics.

Experimental Section

(1) Chemistry

General Methods. FTU-11 was purchased from a chemical library once available through the University of Cincinnati (Cincinnati, OH, USA) and purified by HPLC. FDN-4E, FH535 and Y3 were synthesized as previously described [17, 18, 35]. Solvents were used from commercial vendors without further purification unless otherwise noted. Nuclear magnetic resonance spectra were determined in DMSO-d_6 using Varian instruments (^{1}H, 400; ^{13}C, 100Mz; Varian, Inc., Palo Alto, CA, USA). High resolution electrospray ionization (ESI) mass spectra were recorded on a LTQ-Orbitrap Velos mass spectrometer (Thermo Fisher Scientific, Waltham, MA, USA). The FT resolution was set at 100,000 (at 400 *m*/*z*). Samples were introduced through direct infusion using a syringe pump with a flow rate of 5 μL/min. Melting points were determined in open capillarity tubes with a Büchi B-535 melting point apparatus (Büchi Corp., New Castle, DE, USA) and are uncorrected. Purity was established by combustion analyses performed by Atlantic Microlabs, Inc. (Norcross, GA, USA). Further confirmation of purity of all tested compounds was obtained by RP-HPLC that was performed on an Agilent Technologies 1260 Infinity HPLC system by using the following general method: flow rate = 0.5 mL/min; λ = 254 nm; column = Vydac 201SP C18, 250 mm × 4.6 mm, 90 Å, 5 μm. Eluent A: H_2O + 0.1% TFA (v/v); Eluent B: acetonitrile; gradient profile, starting from 5% B, increasing from 5% B to 100% B over 10 min, holding at 100% B from 10 to 20 min, and decreasing from 100% B to 5% B from 20 to 23 min. Prior to each injection,

the HPLC column was equilibrated for 10 min with 1% B. All compounds tested were determined to be ≥97% pure. Other chemicals were purchased from Sigma-Aldrich (St. Louis, MO, USA) or Fisher Scientific (Pittsburgh, PA, USA) with purify >95%.

1-(1,1,1-Trifluoro-2-(trifluoromethyl)butan-2-yl)-3-(5-(trifluoromethyl)-1,3,4-thiadiazol-2-yl)urea (FTU-11). The purity of **FTU-11** was confirmed by RP-HPLC: R_t = 19.79 min (99% pure; Supporting Information, Figure S1).

1-(4-(Trifluoromethyl)phenyl)-3-(3,4,5-trifluorophenyl)urea (FDN-4E). To a stirred solution of 77 mg (0.52 mmol) of 3,4,5-trifluoroaniline in 3 mL of benzene was added 97 mg (0.52 mmol, 1 eq) of 1-isocyanato-4-(trifluoromethyl)benzene. The mixture was stirred at 50°C for 3 h and was cooled to 25°C. A precipitate was collected by filtration to provide 90 mg (52%) of analytically pure FDN-4E as a white solid: mp 241-242°C. ^{1}H NMR: δ 9.29 (s, 1H, NH), 9.14 (s, 1H, NH), 7.67 (d, 2H, J=8.8Hz), 7.62 (d, 2H, J=8.8Hz), 7.42-7.38 (m, 2H). ^{13}C NMR: δ 152.12 , 150.17 (ddd, *J* = 243.5, 9.9, 5.6 Hz), 142.95 (d, *J* = 1.2 Hz), 135.86 (td, *J* = 12.1, 3.5 Hz), 135.17 (t, *J* = 15.7 Hz), 132.75 (t, *J* = 15.8 Hz), 128.52 , 126.07 (q, *J* = 3.8 Hz), 125.82 , 123.12 , 122.22 (q, *J* = 32.0 Hz), 120.42 , 118.22 , 102.71 (dd). HRMS (ESI) Calcd for $C_{14}H_9F_6N_2O$ [MH^+]: 335.0614. Found: 335.0619. Anal. Calcd for $C_{14}H_8F_6N_2O$: C, 50.31; H, 2.41. Found: C, 50.09; H, 2.49. The purity of **FDN-4E** was further confirmed by RP-HPLC: R_t = 20.3 min (99% pure; Supporting Information, Figure S2).

2,5-Dichloro-*N*-(2-methyl-4-nitrophenyl)benzenesulfonamide (FH535). This compound was synthesized as previously described [35]. The purity of **FH535** was confirmed by RP-HPLC: R_t = 19.5 min (97% pure; Supporting Information, Figure S3).

2,5-Dichloro-*N*-methyl-*N*-(2-methyl-4-nitrophenyl)benzenesulfonamide (FH535-M). To a stirred solution of 360 mg (1 mmol, 1 eq) of FH535 and 830 mg (6 mmol, 6 eq) of potassium carbonate in 2 mL of DMF was slowly added 0.12 mL (2 mmol, 2 eq) of methyl iodide. After stirring at 25°C for 20 h, the mixture was poured into brine, extracted with dichloromethane, dried over anhydrous $MgSO_4$, and evaporated under reduced pressure to afford a crude product. Purification by preparative layer silica gel chromatography using 1:10 (v/v) ethyl acetate-hexane provided 0.2 g (54%) of FH-535-M: mp 142-143°C. ^{1}H NMR: δ 8.23 (d, *J* = 2.7 Hz, 1H), 8.02 (dd, *J* = 8.7, 2.8 Hz, 1H), 7.87-7.77 (m, 3H), 7.26 (d, *J* = 8.7 Hz, 1H), 3.3 (s, 3H), 2.38 (s, 3H). ^{13}C NMR: δ 146.87, 144.7, 140.33, 137.41, 134.79, 134.33, 132.38, 131.05, 130.2, 129.9, 126.05, 121.97, 39.39, 17.84. HRMS (ESI) Calcd for $C_{14}H_{13}Cl_2N_2O_4S$ [MH+]: 374.9968. Found: 374.9968. Anal. Calcd for $C_{14}H_{12}Cl_2N_2O_4S$: C, 44.81; H, 3.22; N, 7.47. Found: C, 44.71; H, 3.17; N, 7.41. The purity of **FH535-M** was confirmed by RP-HPLC: R_t = 20.26 min (99% pure; Supporting Information, Figure S4).

2,5-Dichloro-*N*-(4-nitronaphthalen-1-yl)benzenesulfonamide (Y3). To a suspension of 2.5 mmol (2.5 eq) of sodium hydride (60% dispersion in oil) in 5 mL of anhydrous tetrahydrofuran (THF) was added a solution of 188 mg (1 mmol) of 4-nitro-1-naphthylamine in 1 mL of THF. The mixture was stirred for 10 min at 0°C and 246 mg

(1 mmol) of 2,5-dichlorobenzenesulfonyl chloride was added. The mixture was stirred for 12 h at 25°C, quenched with saturated $NaHCO_3$ and extracted with ethyl acetate. The combined organic layers were washed with brine, dried over anhydrous $MgSO_4$ and concentrated in vacuum to provide crude product. Purification by recrystallization from methanol provided 254 mg (64%) of **Y3**: mp 232-233°C. ^{1}H NMR: δ 11.45 (br s, 1H), 8.41 (d, 2H, J=8.8Hz), 8.27 (d, 1H, J=8.4Hz), 7.94 (d, 1H, J=2.4Hz), 7.82-7.78 (m, 1H), 7.75-7.68 (m, 3H), 7.45 (dd, 1H, J=8.4 and 2.6Hz). ^{13}C NMR: δ 143.38, 138.47, 138.11, 134.62, 133.88, 132.30, 130.35, 129.92, 129.67, 128.37, 127.62, 125.23, 124.73, 123.69, 122.74, 118.96. HRMS (ESI) Calcd for $C_{16}H_9Cl_2N_2O_4S$ [MH-]: 394.9666. Found: 394.9662. Anal. Calcd for $C_{16}H_{10}Cl_2N_2O_4S$: C, 48.38; H, 2.54. Found: C, 48.63; H, 2.46. The purity of **Y3** was confirmed by RP-HPLC: R_t = 19.82 min (99% pure; Supporting Information, Figure S5).

2,5-Dichloro-*N*-methyl-*N*-(4-nitronaphthalen-1-yl)benzenesulfonamide Y3-M. To a solution of 100 mg (0.25 mmol, 1 eq.) of Y3 and 210 mg (6 mmol, 6 eq) of potassium carbonate in 2 mL of DMF was slowly added 0.031 mL (2 mmol, 2 eq) of methyl iodide. After stirring at 25°C for 20 h, the mixture was poured into brine and extracted with dichloromethane. The combined organic layers were dried over anhydrous $MgSO_4$ and evaporated under reduced pressure to afford a crude product. Purification by preparative layer silica gel chromatography using 1:10 ethyl acetate-hexane (v/v) provided 70 mg (68%) of Y3-M: ^{1}H NMR: δ 8.32 (dd, J = 8.8 Hz, 2.8 Hz, 1H), 8.25 (d, J = 8 Hz, 1H), 8.21 (d, J = 8 Hz, 1H), 7.86-7.8 (m, 5H), 7.46 (d, J = 8 Hz, 1H), 3.48 (s, 3H). Anal. Calcd for $C_{17}H_{12}Cl_2N_2O_4S$: C, 49.65; H, 2.94; N, 6.81. Found: C, 49.78; H, 2.88; N,

6.73. The purity of **Y3-M** was confirmed by RP-HPLC: R_t = 20.7 min (99% pure; Supporting Information, Figure S6).

(2) Biology

Cell culture. LS174T colon cancer cells were cultured in EMEM (ATCC, 30-2003) containing 10% (v/v) Fetal Bovine Serum (Sigma F0926, Sigma Aldrich Corp., St. Louis, MO, USA). The DLD-1, SW480 and SW620 colon cancer cells were cultured in DMEM (Sigma D6429) containing 10% (v/v) Fetal Bovine Serum (Sigma, F0926). For proliferation assays, cells ($3.5x10^4$ cells per well) were split into 12-well plates. After 24 h, 1 μL of each compound in DMSO solution were added to each well. DMSO was used as a control. Each experiment was done in triplicate. Cell viability and number were analyzed using the Vi-Cell XR Cell Viability Analyzer (Beckman Coulter, Indianapolis, IN, USA).

Biochemistry. Western blotting: Cells were lysed in the appropriate volume of lysis buffer: 50 mM HEPES, 100 mM NaCl, 2 mM EDTA, 1% (v/v) glycerol, 50 mM NaF, 1 mM Na_3VO_4, 1% (v/v) Triton X-100, with protease inhibitors. The following antibodies were used: AMPK (Cell Signaling, 2532, Cell Signaling Technologies, Danver, MA, USA), pAMPK (Cell Signaling, 2535), ACC (Cell Signaling, 3676), pACC (Cell Signaling, 11818), Actin (Sigma, A1978). Antibodies for Axin 2, c-Myc and Cyclin D1 have been described previously [36]. ATP analysis: Cells growing in 12-well plates were treated with DMSO or inhibitors in DMSO solution and lysed by adding 1 mL boiling

doubly distilled water. Supernatants were analyzed by luminescence using ATP Determination Kit (Invitrogen, A22066; Thermo Fisher Scientific, Waltham, MA, USA).

Reporter assay. Wnt reporter assay and cell staining assay have been described previously [5, 36]. We subcloned Super 8xTOPFlash (provided by Professor Randall Moon, University of Washington) into the pGL4.83 [*hRlucP*/Puro] Vector and transfected it into HEK293T cells. A stable HEK293T cell line containing the TOPFlash reporter was established using puromycin selection. To screen Wnt inhibitors that block the downstream signaling transduction pathway of β-catenin, we treated the reporter cells with 25 mM LiCl to stabilize β-catenin and activate Wnt signaling. The potential Wnt inhibitors identified from screening were validated by transfecting TOPFlash or FOPFlash plus control renilla reporters into HEK293T cells, and then treating the cells with DMSO or testing compounds in DMSO solution. The Wnt signaling was activated by LiCl or Wnt3A treatment.

Mitochondria Membrane potential assay: DLD-1 and LS174T cells were plated onto 24-well plates and maintained in DMEM (DLD-1) and RPMI1640 (LS174T) with 10% (v/v) (DLD-1) and 5% (v/v) (LS174T) serum for one day. The cells were treated with DMSO or a testing compound in DMSO solution for 2 h, followed by staining with 100 nM tetramethylrhodamine methyl ester perchlorate (TMRM) (Cayman Chemical Company, MI, USA) for 15 min. Cells were rinsed once with PBS and then observed under fluorescence microscopy at 568 nm.

Seahorse assay. Approximately $3x10^4$ cells were seeded in XF96 Cell Culture microplate (80 μL of $3.75x10^5$ cells/mL) for all experiments. On the next day, cell culture media were replaced with either Seahorse XF modified media with 25 mM glucose and 1 mM pyruvate. After media exchange, cells were treated with 1 μM of oligomycin A, 1.0 μM FCCP and mixture of 1.0 μM of rotenone and 1.0 μM of antimycin A in standard mitochondrial stress test conditions. To determine the uncoupler effects, FCCP was replaced with an equal volume of DMSO, or a compound to be tested in DMSO solution. ATP production rate was analyzed using Agilent Seahorse XF Real-Time ATP Rate Assay.

Isolation of Mitochondria from Brain Tissue. A mitochondrial isolation protocol was adapted from the previously described protocols with slight modifications [37, 38]. All the steps were carried out at 4 ^oC or on ice. After mice were euthanized with CO_2 followed by rapid decapitation, whole liver was quickly dissected out on a cold block and homogenized using a Teflon-glass dounce homogenizer containing isolation buffer (215 mM mannitol, 75 mM sucrose, 0.1% BSA, 20 mM HEPES, 1 mM EGTA, adjusted to pH 7.2 with KOH). The homogenate was transferred to a 2 mL-microcentrifuge tube and spun at 1,300 x g for 3 min. The supernatant was transferred to a fresh 2 mL-microcentrifuge tube and spun at 13,000 x g for 10 min. The supernatant was discarded, and the crude mitochondrial pellet was resuspended in a 1.5 mL-microcentrifuge tubes and pelleted again at 10,000 x g for 10 min. The supernatant was discarded, and the mitochondrial pellets were resuspended in isolation buffer to obtain an approximate concentration $\geq$10 mg/mL of mitochondria. The absolute protein concentration was determined using a bicinchoninic acid (BCA) protein

assay kit (Pierce, Cat # 23,227) by recording absorbance at 560 nm on a Biotek Synergy HT plate reader (Winooski, VT, USA).

Mitochondrial Bioenergetics Measurements. Mitochondrial bioenergetic measurements were carried out using a Seahorse XFe96 Extracellular Flux Analyzer (Agilent Technologies, Santa Clara, CA, USA) to measure oxygen consumption rate (OCR) during various states of respiration. The OCR were measured in the presence of different substrates, inhibitors and uncouplers of the electron transport chain using previous methods with slight modifications [37, 38]. The stocks used for the assays were 500 mM pyruvate, 250 mM malate, and 30 mM adenosine diphosphate (ADP), and 1 M succinate (pH for all was adjusted to 7.2). Stock assay solutions of 1 mg/mL (1.26 mM) oligomycin A, 1 mM *N*-(4-(trifluoromethoxy)phenyl)carbonohydrazonoyl dicyanide (FCCP), and 1 mM rotenone were prepared in ethanol. Stock solutions of FH535, Y3, FH535-M, and Y3-M were prepared at 5mM in 100% DMSO. As per the instructions from XFe96 Extracellular Flux kit, the sensor cartridge was hydrated with water and kept at 37^{o}C overnight before the experiment. One hour before the assay was conducted, water was removed from assay plates and XF calibrant was added before re-incubation. The injection ports A to D of the sensor cartridge were loaded with 25 µL of different combinations of the above substrates/inhibitors/uncouplers as follows. Before loading, the stocks were diluted appropriately in the respiration buffer (RB) (125 mM KCl, 0.1% BSA, 20 mM HEPES, 2 mM $MgCl_2$, and 2.5 mM KH_2PO_4; pH 7.2) to get the final concentrations in the respiration chamber of 5 µM pyruvate, 2.5 µM malate, 10 µM of succinate and 1 µM ADP (*via* Port A), 1 µM oligomycin A (*via* Port B), 4 µM FCCP or 5 µM/1 µM FH535 or 5 µM/1 µM

Y3 or 5 μM/1 μM FH535-M or 5 μM/1 μM Y3-M (via Port C) and 0.1 μM antimycin A (*via* Port D) starting with the initial volume of 175 μL RB in the chamber and diluting it to 9X, 10X, 11X and 12X with every injection through ports A to D, respectively. Once loaded, the sensor cartridge was placed into the Seahorse XFe96 Flux Analyzer for automated calibration. Seahorse Standard XFe96 assay plates were used for loading mitochondria. Initially total mitochondria were diluted to 6 μg/30 μL in RB and 30 μL was loaded in each well resulting in 6 μg mitochondria/well. The assay plates were centrifuged at 3,000 rpm for 4 min at 4°C to adhere liver mitochondria at the bottom of the wells. After centrifugation, 145 μL RB (pre-incubated to 37 °C) was added without disturbing the mitochondrial layer to obtain a final volume of 175 μL per well. After the instrument calibration with the sensor cartridge was complete, the utility plate was replaced by the plate loaded with mitochondria for bioenergetics analysis. The assays were carried out under a previously optimized protocol. Briefly, it involved cyclic steps of mixing, sequential injections of substrates/inhibitors *via* Ports A thru D, mixing, equilibration, and measurement of the OCR through fluorimetric optical probes. The data output gives State III respiration mediated through complex I and II in the presence of pyruvate, malate (PM), succinate and ADP (Port A) followed by State IV rate in presence of oligomycin (Port B). OCR was then measured in the presence of FCCP or compounds of interest in this study to examine mitochondrial specific uncoupling activity State V_{CI+CII} (Port C) and finally non-mitochondrial respiration in presence of Antimycin A (Port D).

Statistics. All experiments were performed with at least three independent repeats. Statistical analysis was performed using GraphPad Prism 7 (GraphPad Software, CA,

USA). For all analyses, the significance of differences among groups was set at $p < 0.05$. Error bars represent standard deviations. The Seahorse results were analyzed with Seahorse Wave Desktop Software.

Acknowledgments

We are grateful to Professor Randall Moon for the Super 8x TOPFlash and 8x FOPFlash plasmids. CL and DSW were supported by NIH R01 CA172379 from the National Institutes of Health and by NIH UL1 TR000117 from the National Institutes of Health to the University of Kentucky's Center for Clinical and Translational Science. BME was supported by NIH P30 CA177558 from the National Institutes of Health. DSW was also supported in part by the Office of the Dean of the College of Medicine, the Center for Pharmaceutical Research and Innovation in the College of Pharmacy, the Department of Defense (DoD Prostate Cancer Research Program Award W81XWH-16-1-0635 [Grant Log# PC150326P2]), and NIH P30 RR020171 from the National Institute of General Medical Sciences to L. Hersh. VMS was supported by grant IRG 16-182-28 from the American Cancer Society). The Redox Metabolism Shared Resource Facility (RM SRF) that performed the Seahorse XF studies is supported by Markey Cancer Center (P30 CA177558).

Conflict of Interest Statement

CL and DSW have partial ownership in a for-profit venture, Epionc, Inc., that seeks to develop small-molecule inhibitors for cancer treatment. In accord with University of Kentucky policies, CL and DSW have disclosed this work to the University of Kentucky's Intellectual Property Committee and to a Conflict of Interest Oversight Committee.

Ancillary Information

a. Supporting Information Availability:

Supplemental Figures S1-S6 and Molecular Formula Strings Page.

b. Corresponding Author Information:

Correspondence to: chunming.liu@uky.edu or dwatt@uky.edu

c. **List of Abbreviations Used:**

ACC: Acetyl-CoA carboxylase;

AMPK: Adenosine 5' monophosphate-activated protein kinase;

BCA, Bicinchoninic acid;

CRC: colorectal cancer

2DG: 2-deoxy-D-glucose;

DMEM, Dulbecco's Modified Eagle Medium

DMF, Dimethylformamide;

DMSO, Dimethyl sulfoxide;

EDTA, Ethylenediaminetetraacetic acid;

EMEM, Eagle's minimum essential medium;

FDN-4E, 1-(4-(Trifluoromethyl)phenyl)-3-(3,4,5-trifluorophenyl)urea;

FH535, 2,5-Dichloro-*N*-(2-methyl-4-nitrophenyl)benzenesulfonamide

FH535-M, 2,5-Dichloro-*N*-methyl-*N*-(2-methyl-4-nitrophenyl)benzenesulfonamide

FTU-11, 1-(1,1,1-Trifluoro-2-(trifluoromethyl)butan-2-yl)-3-(5-(trifluoromethyl)-1,3,4-thiadiazol-2-yl)urea;

HEPES, 4-(2-Hydroxyethyl)-1-piperazineethanesulfonic acid;

OCR: oxygen consumption rate;

OXPHOS: oxidation/phosphorylation;

RB, respiration buffer;

RP-HPLC, reverse phase high pressure liquid chromatography;

R_t, retention time;

TMRM, Tetramethylrhodamine methyl ester;

Y3, 2,5-Dichloro-*N*-(4-nitronaphthalen-1-yl)benzenesulfonamide;

Y3-M, 2,5-Dichloro-*N*-methyl-*N*-(4-nitronaphthalen-1-yl)benzenesulfonamide.

References

1. Ahmed, K.; Shaw, H. V.; Koval, A.; Katanaev, V. L. A Second WNT for Old Drugs: Drug Repositioning against WNT-Dependent Cancers. *Cancers (Basel)* **2016,** 8, 66-93.
2. Krishnamurthy, N.; Kurzrock, R. Targeting the Wnt/Beta-Catenin Pathway in Cancer: Update on Effectors and Inhibitors. *Cancer Treat Rev* **2018,** 62, 50-60.
3. Nusse, R.; Clevers, H. Wnt/beta-Catenin Signaling, Disease, and Emerging Therapeutic Modalities. *Cell* **2017,** 169, 985-999.
4. Zimmerli, D.; Hausmann, G.; Cantu, C.; Basler, K. Pharmacological Interventions in the Wnt Pathway: Inhibition of Wnt Secretion Versus Disrupting the Protein-Protein Interfaces of Nuclear Factors. *Br J Pharmacol* **2017,** 174, 4600-4610.
5. Shi, J.; Liu, Y.; Xu, X.; Zhang, W.; Yu, T.; Jia, J.; Liu, C. Deubiquitinase USP47/UBP64E Regulates Beta-Catenin Ubiquitination and Degradation and Plays a Positive Role in Wnt Signaling. *Mol Cell Biol* **2015,** 35, 3301-3311.
6. Kahn, M. Can We Safely Target the WNT Pathway? *Nat Rev Drug Discov* **2014,** 13, 513-532.
7. Liu, C.; Li, Y.; Semenov, M.; Han, C.; Baeg, G. H.; Tan, Y.; Zhang, Z.; Lin, X.; He, X. Control of Beta-Catenin Phosphorylation/Degradation by a Dual-Kinase Mechanism. *Cell* **2002,** 108, 837-847.
8. Liu, C.; Kato, Y.; Zhang, Z.; Do, V. M.; Yankner, B. A.; He, X. Beta-Trcp Couples Beta-Catenin Phosphorylation-Degradation and Regulates Xenopus Axis Formation. *Proc Natl Acad Sci U S A* **1999,** 96, 6273-6278.
9. Liu, C.; He, X. Destruction of a Destructor: a New Avenue for Cancer Therapeutics Targeting the Wnt Pathway. *J Mol Cell Biol* **2010,** 2, 70-73.
10. Chung, N.; Marine, S.; Smith, E. A.; Liehr, R.; Smith, S. T.; Locco, L.; Hudak, E.; Kreamer, A.; Rush, A.; Roberts, B.; Major, M. B.; Moon, R. T.; Arthur, W.; Cleary, M.; Strulovici, B.; Ferrer, M. A 1,536-Well Ultra-High-Throughput SiRNA Screen to Identify Regulators of the Wnt/Beta-Catenin Pathway. *Assay Drug Dev Technol* **2010,** 8, 286-294.
11. James, R. G.; Davidson, K. C.; Bosch, K. A.; Biechele, T. L.; Robin, N. C.; Taylor, R. J.; Major, M. B.; Camp, N. D.; Fowler, K.; Martins, T. J.; Moon, R. T. WIKI4, a Novel Inhibitor of Tankyrase and Wnt/Beta-Catenin Signaling. *PLoS One* **2012,** 7, e50457.
12. Wang, X.; Moon, J.; Dodge, M. E.; Pan, X.; Zhang, L.; Hanson, J. M.; Tuladhar, R.; Ma, Z.; Shi, H.; Williams, N. S.; Amatruda, J. F.; Carroll, T. J.; Lum, L.; Chen, C. The Development of Highly Potent Inhibitors for Porcupine. *J Med Chem* **2013,** 56, 2700-2704.
13. Huang, S. M.; Mishina, Y. M.; Liu, S.; Cheung, A.; Stegmeier, F.; Michaud, G. A.; Charlat, O.; Wiellette, E.; Zhang, Y.; Wiessner, S.; Hild, M.; Shi, X.; Wilson, C. J.; Mickanin, C.; Myer, V.; Fazal, A.; Tomlinson, R.; Serluca, F.; Shao, W.; Cheng, H.; Shultz, M.; Rau, C.; Schirle, M.; Schlegl, J.; Ghidelli, S.; Fawell, S.; Lu, C.; Curtis, D.; Kirschner, M. W.; Lengauer, C.; Finan, P. M.; Tallarico, J. A.; Bouwmeester, T.; Porter, J. A.; Bauer, A.; Cong, F. Tankyrase Inhibition Stabilizes Axin and Antagonizes Wnt Signalling. *Nature* **2009,** 461, 614-620.
14. Emami, K. H.; Nguyen, C.; Ma, H.; Kim, D. H.; Jeong, K. W.; Eguchi, M.; Moon, R. T.; Teo, J. L.; Kim, H. Y.; Moon, S. H.; Ha, J. R.; Kahn, M. A Small Molecule Inhibitor of Beta-Catenin/CREB-Binding Protein Transcription [Corrected]. *Proc Natl Acad Sci U S A* **2004,** 101, 12682-12687.
15. Burikhanov, R.; Sviripa, V. M.; Hebbar, N.; Zhang, W.; Layton, W. J.; Hamza, A.; Zhan, C. G.; Watt, D. S.; Liu, C.; Rangnekar, V. M. Arylquins Target Vimentin to Trigger Par-4 Secretion for Tumor Cell Apoptosis. *Nat Chem Biol* **2014,** 10, 924-926.
16. Zhang, W.; Sviripa, V.; Chen, X.; Shi, J.; Yu, T.; Hamza, A.; Ward, N. D.; Kril, L. M.; Vander Kooi, C. W.; Zhan, C. G.; Evers, B. M.; Watt, D. S.; Liu, C. Fluorinated N,N-Dialkylaminostilbenes Repress Colon Cancer by Targeting Methionine S-Adenosyltransferase 2A. *ACS Chem Biol* **2013,** 8, 796-803.
17. Kenlan, D. E.; Rychahou, P.; Sviripa, V. M.; Weiss, H. L.; Liu, C.; Watt, D. S.; Evers, B. M. Fluorinated N,N'-Diarylureas as Novel Therapeutic Agents Against Cancer Stem Cells. *Mol Cancer Ther* **2017,** 16, 831-837.
18. Sviripa, V.; Zhang, W.; Conroy, M. D.; Schmidt, E. S.; Liu, A. X.; Truong, J.; Liu, C.; Watt, D. S. Fluorinated N,N'-Diarylureas as AMPK Activators. *Bioorg Med Chem Lett* **2013,** 23, 1600-1603.
19. Handeli, S.; Simon, J. A. A Small-Molecule Inhibitor of Tcf/Beta-Catenin Signaling Down-Regulates PPARgamma and PPARdelta Activities. *Mol Cancer Ther* **2008,** 7, 521-529.

20. Zhou, G.; Myers, R.; Li, Y.; Chen, Y.; Shen, X.; Fenyk-Melody, J.; Wu, M.; Ventre, J.; Doebber, T.; Fujii, N.; Musi, N.; Hirshman, M. F.; Goodyear, L. J.; Moller, D. E. Role of AMP-Activated Protein Kinase in Mechanism of Metformin Action. *J Clin Invest* **2001,** 108, 1167-1174.
21. Goransson, O.; McBride, A.; Hawley, S. A.; Ross, F. A.; Shpiro, N.; Foretz, M.; Viollet, B.; Hardie, D. G.; Sakamoto, K. Mechanism of Action of A-769662, a Valuable Tool for Activation of AMP-Activated Protein Kinase. *J Biol Chem* **2007,** 282, 32549-32560.
22. Hardie, D. G.; Ross, F. A.; Hawley, S. A. AMPK: a Nutrient and Energy Sensor that Maintains Energy Homeostasis. *Nat Rev Mol Cell Biol* **2012,** 13, 251-262.
23. Kim, J.; Yang, G.; Kim, Y.; Kim, J.; Ha, J. AMPK Activators: Mechanisms of Action and Physiological Activities. *Exp Mol Med* **2016,** 48, e224.
24. Brand, M. D.; Nicholls, D. G. Assessing Mitochondrial Dysfunction in Cells. *Biochem J* **2011,** 435, 297-312.
25. Turcios, L.; Vilchez, V.; Acosta, L. F.; Poyil, P.; Butterfield, D. A.; Mitov, M.; Marti, F.; Gedaly, R. Sorafenib and FH535 in Combination Act Synergistically on Hepatocellular Carcinoma by Targeting Cell Bioenergetics and Mitochondrial Function. *Dig Liver Dis* **2017,** 49, 697-704.
26. Bordwell, F. G. Equilibrium Acidities in Dimethyl Sulfoxide Solution. *Acct. Chem. Res.* **1988,** 21, 456-463.
27. Porcelli, A. M.; Ghelli, A.; Zanna, C.; Pinton, P.; Rizzuto, R.; Rugolo, M. PH Difference Across the Outer Mitochondrial Membrane Measured with a Green Fluorescent Protein Mutant. *Biochem Biophys Res Commun* **2005,** 326, 799-804.
28. Lou, P. H.; Hansen, B. S.; Olsen, P. H.; Tullin, S.; Murphy, M. P.; Brand, M. D. Mitochondrial Uncouplers with an Extraordinary Dynamic Range. *Biochem J* **2007,** 407, 129-140.
29. Wick, A. N.; Drury, D. R.; Nakada, H. I.; Wolfe, J. B. Localization of the Primary Metabolic Block Produced by 2-Deoxyglucose. *J Biol Chem* **1957,** 224, 963-969.
30. Barker, N.; Hurlstone, A.; Musisi, H.; Miles, A.; Bienz, M.; Clevers, H. The Chromatin Remodelling Ractor Brg-1 Interacts with Beta-Catenin to Promote Target Gene Activation. *EMBO J* **2001,** 20, 4935-4943.
31. Fagotto, F.; Gluck, U.; Gumbiner, B. M. Nuclear Localization Signal-Independent and Importin/Karyopherin-Independent Nuclear Import of Beta-Catenin. *Curr Biol* **1998,** 8, 181-190.
32. Holik, A. Z.; Young, M.; Krzystyniak, J.; Williams, G. T.; Metzger, D.; Shorning, B. Y.; Clarke, A. R. Brg1 Loss Attenuates Aberrant Wnt-Signalling and Prevents Wnt-Dependent Tumourigenesis in the Murine Small Intestine. *PLoS Genet* **2014,** 10, e1004453.
33. Costa, R.; Peruzzo, R.; Bachmann, M.; Monta, G. D.; Vicario, M.; Santinon, G.; Mattarei, A.; Moro, E.; Quintana-Cabrera, R.; Scorrano, L.; Zeviani, M.; Vallese, F.; Zoratti, M.; Paradisi, C.; Argenton, F.; Brini, M.; Cali, T.; Dupont, S.; Szabo, I.; Leanza, L. Impaired Mitochondrial ATP Production Downregulates Wnt Signaling via ER Stress Induction. *Cell Rep* **2019,** 28, 1949-1960 e1946.
34. Brown, K.; Yang, P.; Salvador, D.; Kulikauskas, R.; Ruohola-Baker, H.; Robitaille, A. M.; Chien, A. J.; Moon, R. T.; Sherwood, V. WNT/Beta-Catenin Signaling Regulates Mitochondrial Activity to Alter the Oncogenic Potential of Melanoma in a PTEN-Dependent Manner. *Oncogene* **2017,** 36, 3119-3136.
35. Kril, L. M.; Vilchez, V.; Jiang, J.; Turcios, L.; Chen, C.; Sviripa, V. M.; Zhang, W.; Liu, C.; Spear, B.; Watt, D. S.; Gedaly, R. N-Aryl Benzenesulfonamide Inhibitors of [3H]-Thymidine Incorporation and Beta-Catenin Signaling in human Hepatocyte-Derived Huh-7 Carcinoma Cells. *Bioorg Med Chem Lett* **2015,** 25, 3897-3899.
36. Zhang, W.; Sviripa, V.; Kril, L. M.; Chen, X.; Yu, T.; Shi, J.; Rychahou, P.; Evers, B. M.; Watt, D. S.; Liu, C. Fluorinated N,N-Dialkylaminostilbenes for Wnt Pathway Inhibition and Colon Cancer Repression. *J Med Chem* **2011,** 54, 1288-1297.
37. Hubbard, W. B.; Joseph, B.; Spry, M.; Vekaria, H. J.; Saatman, K. E.; Sullivan, P. G. Acute Mitochondrial Impairment Underlies Prolonged Cellular Dysfunction after Repeated Mild Traumatic Brain Injuries. *J Neurotrauma* **2019,** 36, 1252-1263.
38. Hubbard, W. B.; Harwood, C. L.; Geisler, J. G.; Vekaria, H. J.; Sullivan, P. G. Mitochondrial Uncoupling Prodrug Improves Tissue Sparing, Cognitive Outcome, and Mitochondrial Bioenergetics After Traumatic Brain Injury in Male Mice. *J Neurosci Res* **2018,** 96, 1677-1688.

Figure Legends

Fig. 1. Identification of urea derivatives as novel Wnt inhibitors. **A**. Structures of 1-(1,1,1,4,4,4-hexafluoro-2-(trifluoromethyl)butan-2-yl)-3-(5-(trifluoromethyl)-1,3,4-thiadiazol-2-yl)urea (FTU-11) and 1-(4-(trifluoromethyl)phenyl)-3-(3,4,5-trifluorophenyl)urea (FDN-4E). **B** and **C**. Dose-response luciferase study using FTU-11 and FDN-4E in a HEK293T cell line containing TOPFlash reporter. **D**. Effects of FTU-11 and FDN-4E in HEK293T cells transfected with Super 8x TOFFlash or 8x FOPFlash.

Fig. 2. Validating antineoplastic activity and Wnt inhibition activity of FTU-11 and FDN-4E. **A**. Cell proliferation assays using FTU-11 and FDN-4E in LS174T and DLD-1 CRC cells. **B**. Dose response study of FTU-11 and FDN-4E on components of Wnt signaling pathway and downstream targets.

Fig. 3. FTU-11 and FDN-4E activated AMPK in CRC cells. FTU-11 (3 μM) and FDN-4E (3 μM) increased AMPK activity (T172 phosphorylation) and inhibited ACC (S79 phosphorylation).

Figure 4. Linkage between AMPK activation and the inhibition of Wnt signaling. **A**. Compound C (5 μM), an AMPK inhibitor, decreased urea-induced AMPK phosphorylation and ACC phosphorylation. **B**. Failure of Compound C (5 μM) to rescue Wnt signaling inhibited by FTU-11 (3 μM) and FDN-4E (3 μM). Failure of a specific AMPK activator, A769662 (10 μM), to inhibit Wnt signaling. **C**. Increased AMPK

activity caused by A769662 (ACC S79 phosphorylation) without affecting AMPK phosphorylation. **D.** FH535 (3 μM) inhibited Wnt signaling. **E**. FH535 (3 μM) activated AMPK.

Fig. 5. Effects of FTU-11 and FH535 on mitochondrial respiration. **A**. FTU-11 (3 μM) and FH535 (3 μM) and reduced mitochondrial ATP production using mitochondrial uncoupler FCCP (1 μM) as a control. Glycolytic ATP production rates were increased upon uncoupler treatment. **B**. FTU-11 (3 μM) reduced mitochondrial membrane potential. **C**. Uncoupling assay: model of uncoupling effects on Oxygen Consumption rate (OCR). **D-F**. Effects of FCCP (1 μM) or testing compound (3 μM) in uncoupling assays in DLD-1 cells.

Fig. 6. Uncoupler function is linked to AMPK activation and Wnt inhibition. **A**. 2,5-dichloro-*N*-(2-methyl-4-nitrophenyl)benzenesulfonamide (FH535), it active analog Y3 and their *N*-methylation analog FH535-M and Y3-M. **B.** FH535-M (3 μM) failure to induce uncoupling activity (red: FH535; Grey: FH535-M; and Blue: DMSO). **C-F**. FH535-M (3 μM) and Y3-M (3 μM) lost activities in inducing AMPK activation and inhibiting Wnt signaling.

Fig. 7. FH535 and Y3 directly target mitochondria. **A.** Schematic representation of proton uncoupling promoted by FH535**.** **B** and **C.** Uncoupling activities of FCCP (1 μM) and test compounds in purified mitochondria from mouse liver.

Fig. 8. A common mechanism of mitochondria uncoupler and glycolytic inhibitor on AMPK activation and Wnt signaling inhibition. **A** and **B**. Mitochondrial uncoupler FCCP activated AMPK and inhibited Wnt signaling. **C** and **D**. Glycolytic inhibitor 2-DG activated AMPK, inhibited Wnt signaling. E. Effects of 2-DG (10 mM) on ATP levels in LS174T cells. **F**. FTU-11 and FH535 reduced LiCl-induced β-catenin accumulation in LS174T cells.

Cover Fig. Proton uncouplers inhibited mitochondrial ATP production (*i.e.*, ATP↓) that is required for several steps in the Wnt signaling transduction pathway, including β-catenin nucleus translocation and ATP-dependent chromatin remodeling. Increased AMP/ATP ratio also induced AMPK activation (*i.e.*, $AMPK^{P}$) and ACC inhibition (*i.e.*, ACC^{P}).

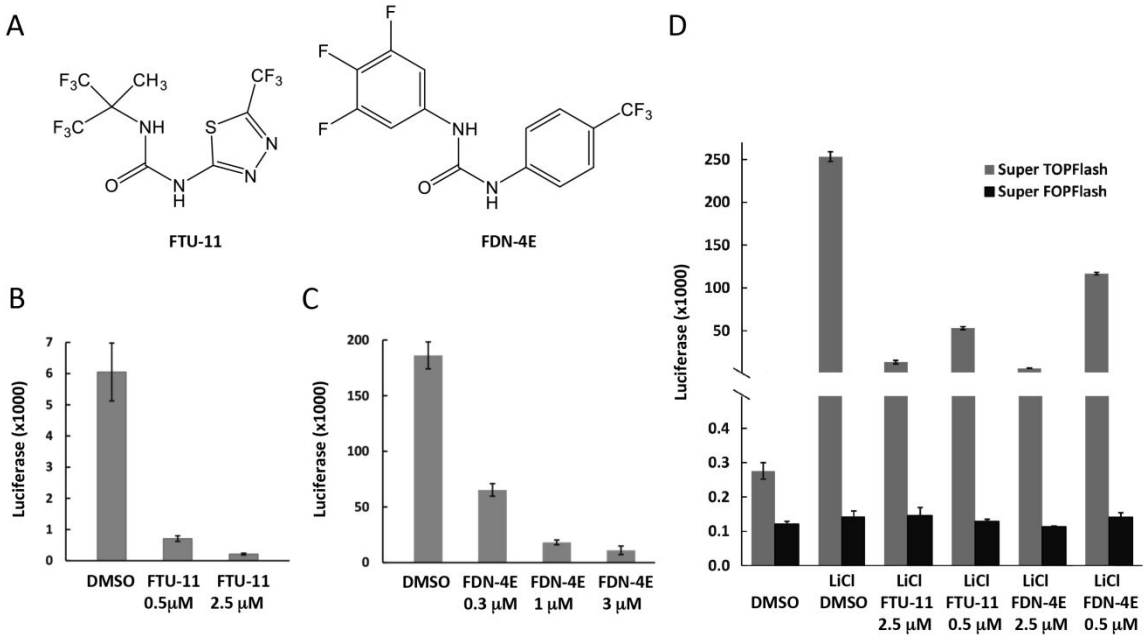
A
FTU-11
FDN-4E
B
Luciferase (x1000)
DMSO
FTU-11 0.5μM
FTU-11 2.5 μM
C
Luciferase (x1000)
DMSO
FDN-4E 0.3 μM
FDN-4E 1 μM
FDN-4E 3 μM
D
Super TOPFlash
Super FOPFlash
Luciferase (x1000)
DMSO
LiCl DMSO
LiCl FTU-11 2.5 μM
LiCl FTU-11 0.5 μM
LiCl FDN-4E 2.5 μM
LiCl FDN-4E 0.5 μM

Figure 1

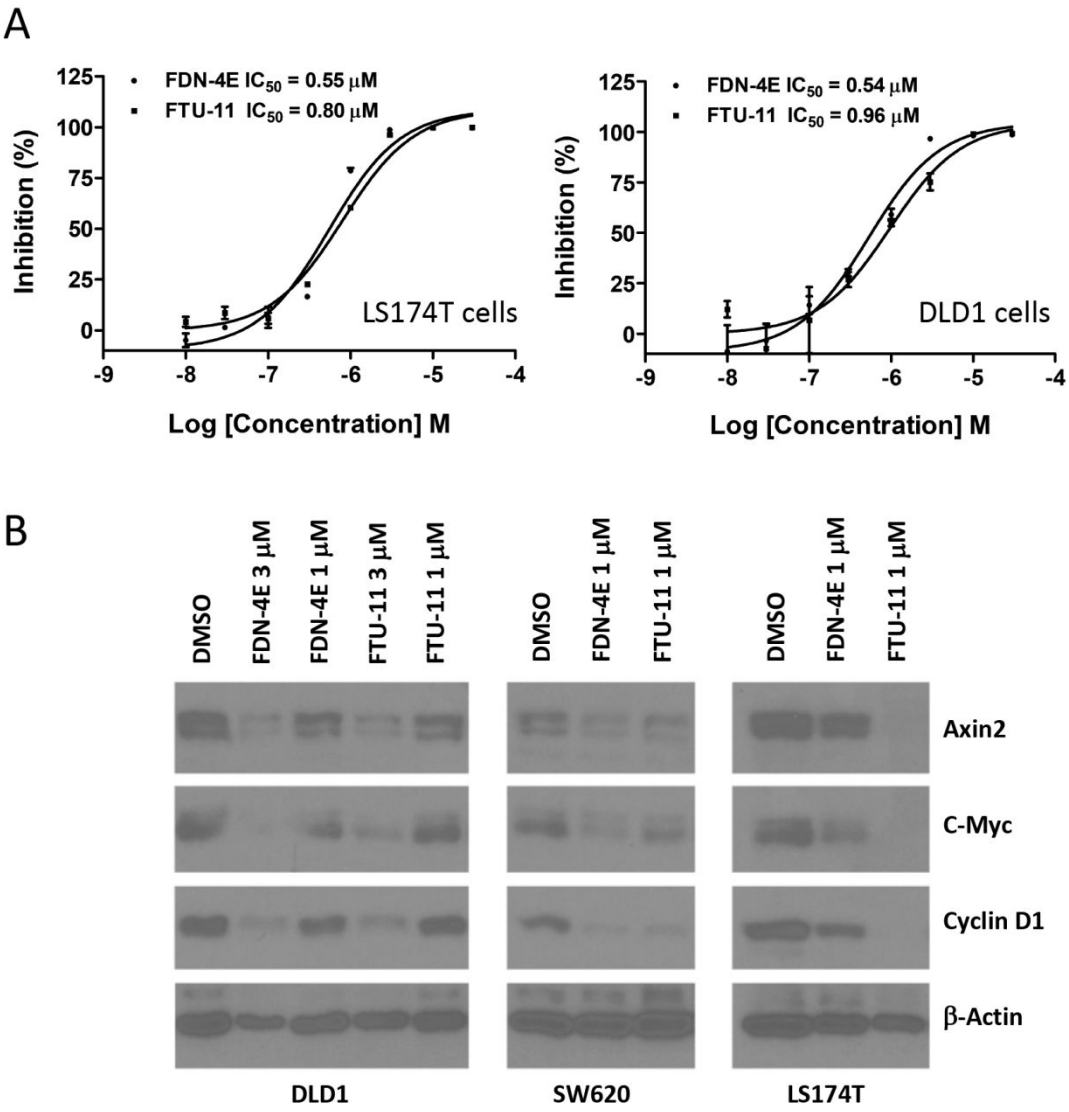
A
FDN-4E IC50 = 0.55 μM
FTU-11 IC50 = 0.80 μM
Inhibition (%)
LS174T cells
Log [Concentration] M
FDN-4E IC50 = 0.54 μM
FTU-11 IC50 = 0.96 μM
Inhibition (%)
DLD1 cells
Log [Concentration] M
B
DMSO
FDN-4E 3 μM
FDN-4E 1 μM
FTU-11 3 μM
FTU-11 1 μM
DMSO
FDN-4E 1 μM
FTU-11 1 μM
DMSO
FDN-4E 1 μM
FTU-11 1 μM
Axin2
C-Myc
Cyclin D1
β-Actin
DLD1
SW620
LS174T

Figure 2

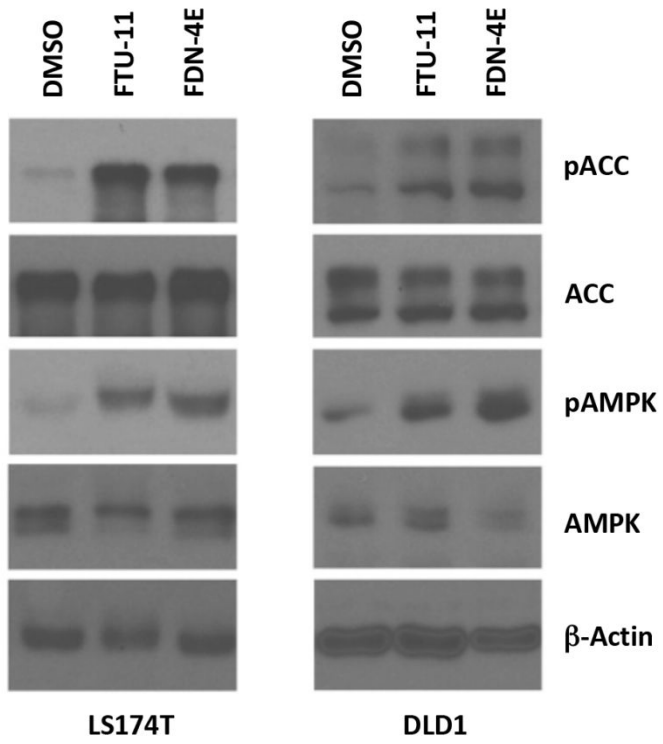
DMSO
FTU-11
FDN-4E
DMSO
FTU-11
FDN-4E
pACC
ACC
pAMPK
AMPK
β-Actin
LS174T
DLD1

Figure 3

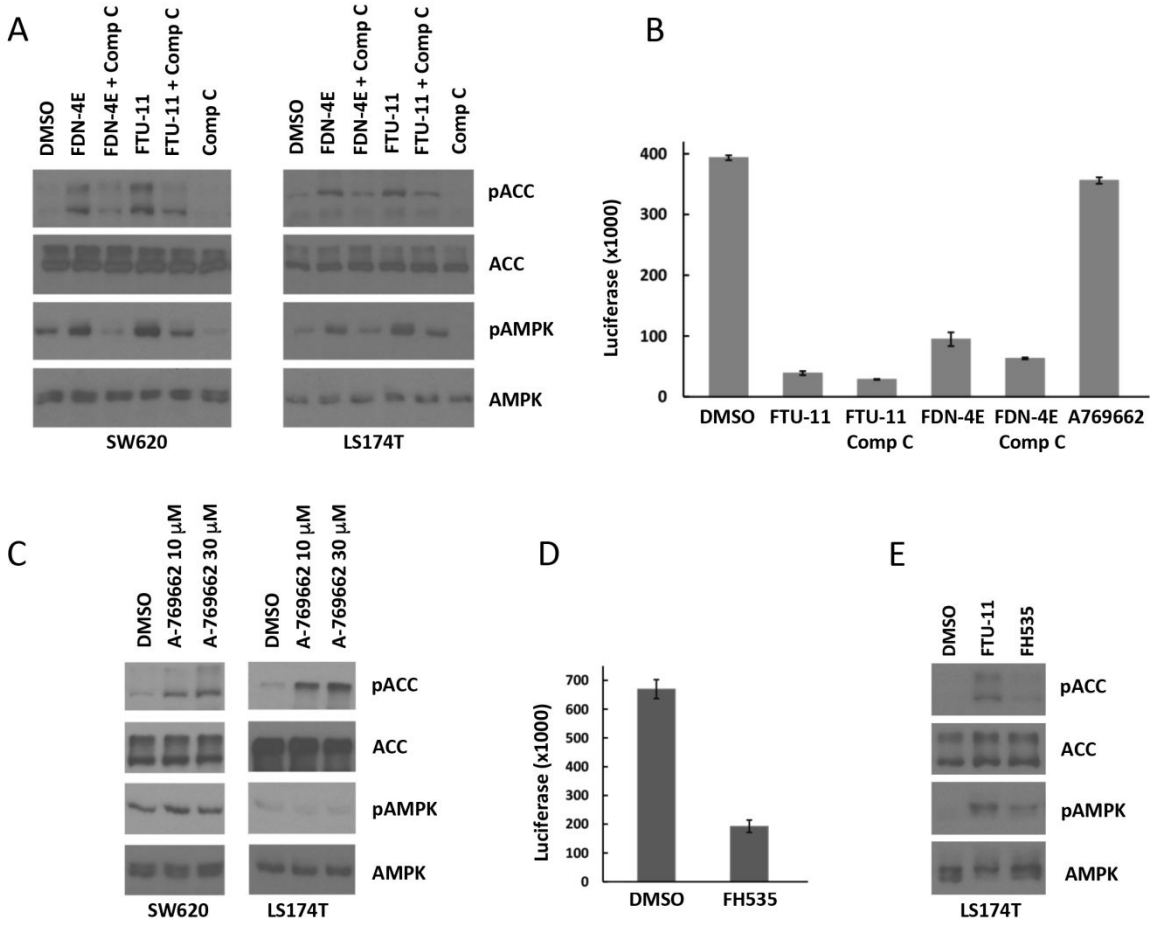
A
DMSO
FDN-4E
FDN-4E + Comp C
FTU-11
FTU-11 + Comp C
Comp C
pACC
ACC
pAMPK
AMPK
SW620
LS174T
B
Luciferase (x1000)
400
300
200
100
0
DMSO
FTU-11
FTU-11 Comp C
FDN-4E
FDN-4E Comp C
A769662
C
DMSO
A-769662 10 μM
A-769662 30 μM
pACC
ACC
pAMPK
AMPK
SW620
LS174T
D
Luciferase (x1000)
700
600
500
400
300
200
100
0
DMSO
FH535
E
DMSO
FTU-11
FH535
pACC
ACC
pAMPK
AMPK
LS174T

Figure 4

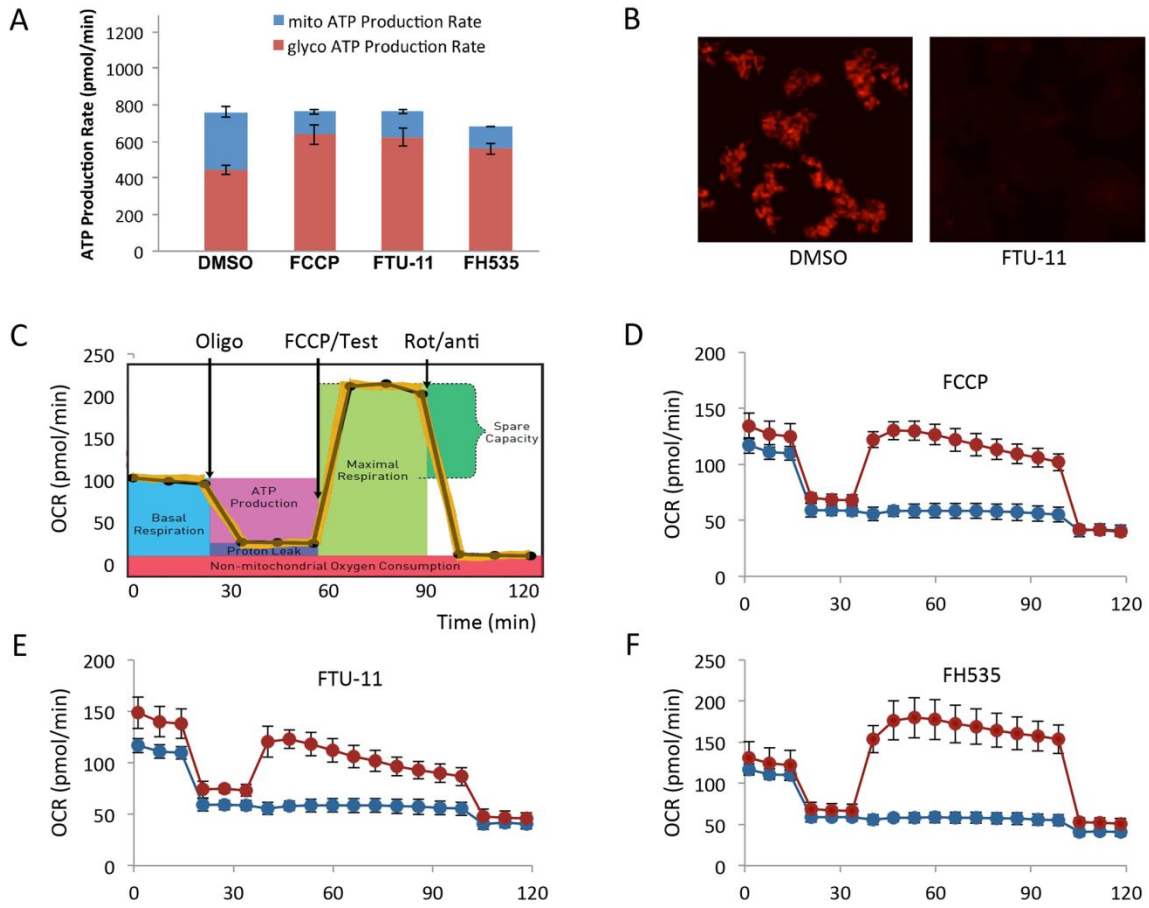
A
mito ATP Production Rate
glyco ATP Production Rate
ATP Production Rate (pmol/min)
1200
1000
800
600
400
200
0
DMSO
FCCP
FTU-11
FH535
B
DMSO
FTU-11
C
Oligo
FCCP/Test
Rot/anti
OCR (pmol/min)
Spare Capacity
Maximal Respiration
ATP Production
Basal Respiration
Proton Leak
Non-mitochondrial Oxygen Consumption
Time (min)
D
FCCP
E
FTU-11
F
FH535

Figure 5

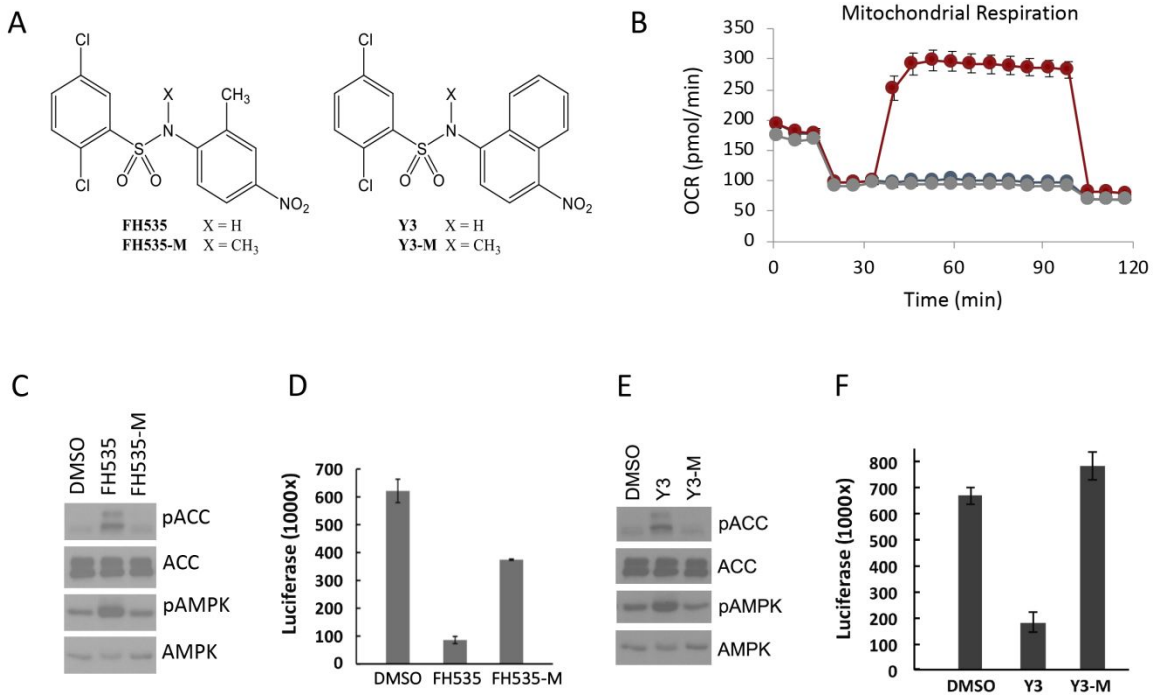
A
Cl
X
CH3
N
S
O
O
Cl
NO2
FH535 X = H
FH535-M X = CH3
Y3 X = H
Y3-M X = CH3
B
Mitochondrial Respiration
OCR (pmol/min)
Time (min)
C
DMSO
FH535
FH535-M
pACC
ACC
pAMPK
AMPK
D
Luciferase (1000x)
DMSO FH535 FH535-M
E
DMSO
Y3
Y3-M
pACC
ACC
pAMPK
AMPK
F
Luciferase (1000x)
DMSO Y3 Y3-M

Figure 6

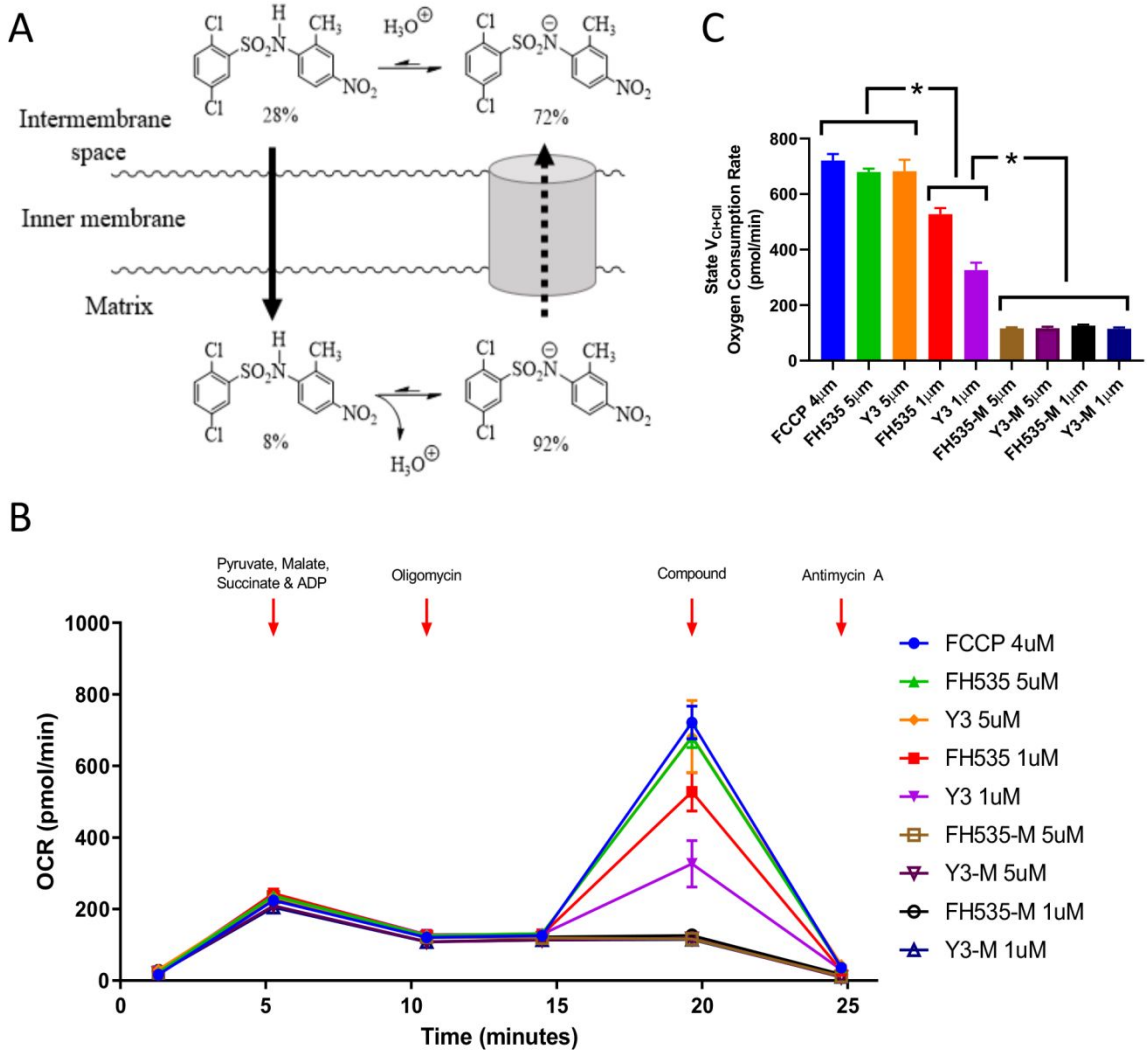
A
Intermembrane space
Inner membrane
Matrix
28%
72%
8%
92%
B
Pyruvate, Malate, Succinate & ADP
Oligomycin
Compound
Antimycin A
OCR (pmol/min)
Time (minutes)
FCCP 4uM
FH535 5uM
Y3 5uM
FH535 1uM
Y3 1uM
FH535-M 5uM
Y3-M 5uM
FH535-M 1uM
Y3-M 1uM
C
State VCI+CII Oxygen Consumption Rate (pmol/min)
FCCP 4μm
FH535 5μm
Y3 5μm
FH535 1μm
Y3 1μm
FH535-M 5μm
Y3-M 5μm
FH535-M 1μm
Y3-M 1μm

Figure 7

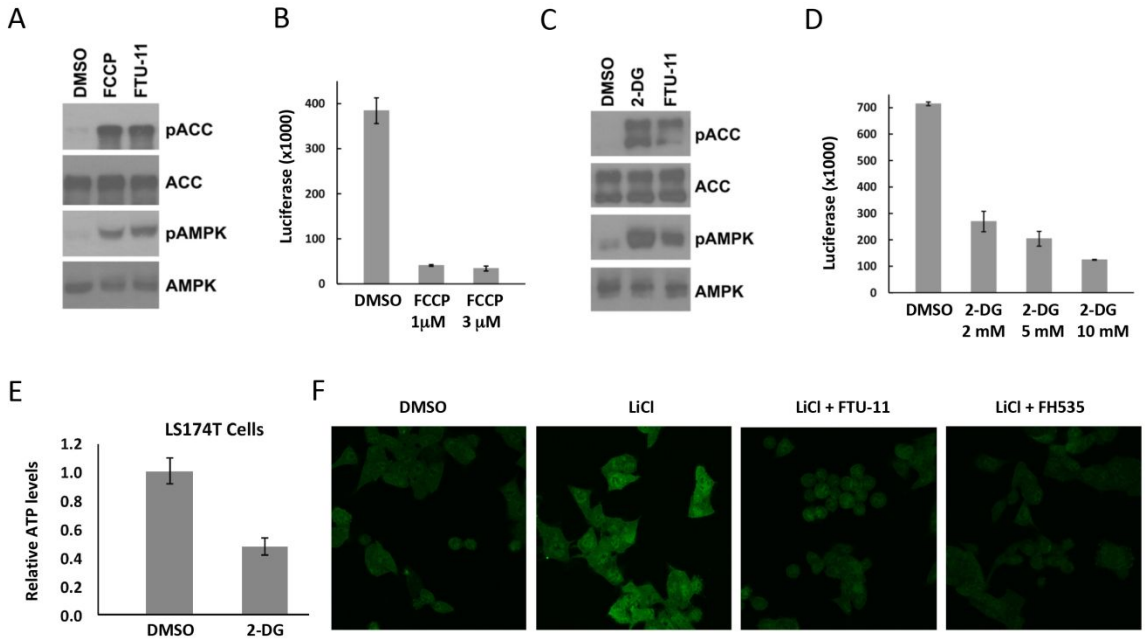
A
DMSO
FCCP
FTU-11
pACC
ACC
pAMPK
AMPK
B
Luciferase (x1000)
400
300
200
100
0
DMSO
FCCP 1μM
FCCP 3 μM
C
DMSO
2-DG
FTU-11
pACC
ACC
pAMPK
AMPK
D
Luciferase (x1000)
700
600
500
400
300
200
100
0
DMSO
2-DG 2 mM
2-DG 5 mM
2-DG 10 mM
E
LS174T Cells
Relative ATP levels
1.2
1.0
0.8
0.6
0.4
0.2
0.0
DMSO
2-DG
F
DMSO
LiCl
LiCl + FTU-11
LiCl + FH535

Figure 8

Table of Contents Graphic